13th International Symposium on Particle Image Velocimetry – ISPIV 2019
Munich, Germany, July 22-24, 2019

Measuring the Sub-Surface Velocity Field in Faraday Flows

Raffaele Colombi*, Michael Schlüter, Alexandra von Kameke

Hamburg University of Technology, Institute of Multiphase Flows, Hamburg, Germany

* raffaele.colombi@tuhh.de

Abstract

Capillary ripples that form on the surface of a fluid being subject to vertical shaking are known as Faraday waves. Although it is well known that the form and shape of the waves pattern depends on driving amplitude and frequency, Faraday (1831), only recent studies discovered the existence of a horizontal velocity field at the surface, called Faraday flow, von Kameke et al. (2011, 2013); Francois et al. (2013). The Faraday flow exhibits attributes of two-dimensional (2D) turbulence, in particular the presence of an inverse energy cascade, by which energy is introduced at intermediate forcing scales and transferred upwards to larger scales, resulting in a net inverse energy flux.
Despite the increasing attention towards the well-validated inverse energy flux in the Faraday flow and other not strictly 2-dimensional systems (as presented in Biferale et al. (2017)), very little is known about the velocity field and its structures developing beneath the fluid surface. This study aims at shedding light on the flow characteristics of the Faraday experiment, with particular focus on the sub-surface velocity fields. Planar velocity fields are measured by means of particle image velocimetry (PIV) with high spatial and temporal resolution at various horizontal planes, in order to characterise the three-dimensional structures of the Faraday flow in dependence of the immersion depth.

1 Introduction

Faraday waves are capillary ripples that form on the surface of a fluid being subject to vertical agitation. The resulting waves are known to be self-organizing into patterns that vary depending on driving amplitude and frequency, Faraday (1831). Because of the strong influence of boundary conditions, Faraday waves are subject to studies for a large variety of applications, ranging from bio-medicine to material sciences (e.g. controlled pattern formation, walking and orbiting of droplets), Saylor and Kinard (2005); Couder et al. (2005).
In capillary ripples, a complex and random transport of floating particles is generated by non-linear interactions at the surface of the Faraday wavefield, such as imperfections and traveling waves, Saylor and Kinard (2005); Ramshankar et al. (1990). However, only recent studies, von Kameke et al. (2011, 2013); Francois et al. (2013), proved the existence of a horizontal velocity field at the surface, called Faraday flow, which was shown to exhibit attributes of two-dimensional (2D) turbulence.
One of the main features of Faraday flows is the presence of an inverse energy cascade. For 3D isotropic turbulence, energy is injected in the flow at large scales, and consequently transported to smaller scales through the vortex stretching mechanism, and finally dissipated through viscous effects. However, numerical and experimental results confirmed the presence of a dual energy cascade in case of 2D-turbulence (von Kameke et al. (2011); Farazmand et al. (2011); Boffetta and Ecke (2012) and references therein), as theoretically predicted by Kraichnan (1971).
Energy is introduced at intermediate forcing scales and transferred upwards to larger scales, resulting in a net inverse energy flux. This phenomenon leads to energy condensation, by which large and ordered flow structures emerge from the the seemingly disordered motion at small scales. In principle, this energy could be exploited as a potential source of renewable energy. Inversely, for wavelengths smaller than the forcing scale, an enstrophy cascade transfers enstrophy to the smaller wavelengths.
Despite the increasing attention towards the well-validated inverse energy flux in Faraday flow and other

not strictly 2-dimensional systems (as presented in Biferale et al. (2017)), and experiments carried out to characterize the 3-dimensional trajectories of the particles at the surface, Francois et al. (2014), very little is known about the flow structures developing beneath the surface.
This preliminary study aims at shedding light on the flow characteristics of the Faraday experiment, with particular focus on the velocities at different depths. The velocity fields are measured by means of planar PIV with high spatial and temporal resolution at different horizontal planes, in order to develop a basis for subsequent and more advanced measurement techniques, by which the three-dimensional structures of the Faraday flow in dependence of the fluid depth will be investigated. Although the analysis cannot provide data to reconstruct the full 3-dimensional components of the velocity field, this preliminary study is expected to be of importance in highlighting regions of interest for future analysis.

2 Materials and Methods

Container and vertical shaking

Faraday waves are investigated in a circular container of acrylic glass (diameter 290 mm) filled with water at 21.5 °C. A depth of 30 mm is chosen for a deep water approximation, such that the depth is larger than the wavelength of the ripples at the surface. The container is vertically shaken by an electromagnetic shaker (TIRA vib). A schematic representation of the experimental set-up is shown in Fig. 1.
Monochromatic forcing at $f_0 = 50$ Hz is imposed to the shaker from a function generator (RIGOL), and the acceleration of the container is measured with an accelerometer (Kistler). The amplitude a of the acceleration was set in order to achieve the onset of unstable behaviour at the surface (threshold acceleration $a_{th} = 0.466$ g), which is read out by a high-frequency digitalizer (Spectrum).

Camera and image acquisition

A second signal from the function generator is used to trigger the high-speed camera (PCO dmax HS2). The camera is synchronised with the dominant frequency of the waves, which is found at the first subharmonic of the driving frequency $f = f_0/2 = 25$ Hz, for a rate corresponding to 400 fps, or eight wave periods. The phase difference between the two signals from the function generator was then carefully monitored through the digitalizer and tuned in order to capture the point of zero amplitude in the waves.
The camera is placed on the side of the shaker supports, and an optical prism-mirror is used to deflect the camera field of view in the vertical direction. At the chosen working distance, the camera resolution of 1400x1050 pixels corresponds to a field of view of approx 7×5 cm^2, slightly varying depending on the measurement depth. Images are saved in 16 bit format (.b16), and subsequently converted back to a 12 bit format, which corresponds to the actual bit depth of the camera.

PIV measurements

Two PIV techniques are used for the measurements at and below the surface respectively, which mainly differ in the choice of light source and particles.
For the measurements beneath the waver level, red fluorescent polyethylene microspheres are used (diameter of 10-45 μm, Cospheric), illuminated by a continuous wave argon laser (wavelength of 457-515 nm, Ion Technologies). An optical arrangement is used to deflect the laser beam (first upwards and later again horizontally) in order to generate a light sheet (60 mm wide, 1 mm thick) and to easily adjust the measuring plane height. The particles have a density of 0.995 g/cm^3 - and uniformly disperse in the water volume, when additionally treated with a surfactant, as described below. A high-precision longpass filter is used to capture the fluorescence of the particles (peak at 607 nm) and simultaneously shield the camera sensor from the laser light. This technique was used to measure the velocity fields at five horizontal planes h, where h is the height from the container floor (h in [5, 25] mm in steps of 5 mm).
However, due to total light refraction at the water level, the combination of laser and fluorescent particles cannot be used to measure the velocity field at the water surface. In this case, a combination of floating hollow glass microspheres (diameter of approx. 70 μm, Fibre Glast) and back-light (LED panel) was preferred instead.
For both PIV techniques, 0.3 g of particles are wetted in a 10%-solids solution with a surfactant (1% Tween 80 solution, Polysorbate 80, non-ionic surfactant). This helps to uniformly disperse the naturally buoyant particles (fluorescent) in the water volume, and the same surfactant is used in all measurements in order to avoid differences in the waves (e.g. due to changes in surface tension).

Fig. 1 provides a schematic representation of the experimental set-up for the two PIV techniques described above.

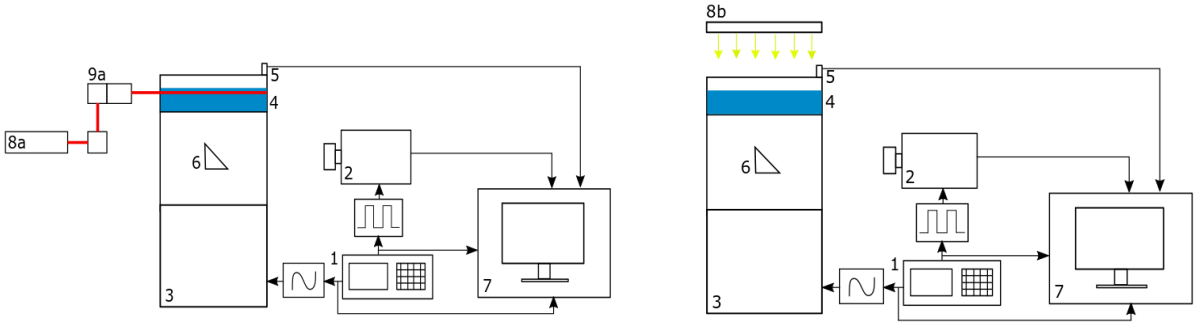

(a) (b)

Figure 1: Schematic representation of the experimental set-up. The function generator (1) triggers the high-speed camera (2) and drives the shaker (3). The acceleration of the water container (4) is measured with an accelerometer (5). A prism-mirror (6) is used to deflect the camera field of view. All the signals are monitored with a digitalizer (7), whereas data is saved on a laboratory laptop. (8a) and (9a) depict the laser and its optics, whereas (8b) shows the LED panel for the backlight PIV.

PIV data evaluation

PIV data is evaluated using PIVview (PIVTEC GmbH, Germany). The images from the surface measurement (LED lighting) are pre-processed by subtracting a background picture of the empty container, in order to remove background noise and improve the contrast. The region of interest (ROI) spans over the entire field of view. The pictures are divided into a grid with interrogation window (IW) of 24×24-pixels. By contrast, the images from the laser lighting (beneath the water surface) are pre-processed by applying a high-pass filter (kernel size of 5.5) in order to reduce the noise coming from particles outside the laser sheet. A coarser grid with an IW of 48×48 pixels is used for the measurement heights below $h = 25$ mm. For both cases, a grid overlap of 50% is introduced to reduce the noise from calculation of differentials.
After an initial evaluation using a standard, single-pass interrogation, a multi-grid interrogation method is used as second-order accurate method, with initial sampling windows of 96×96 pixels. For the sub-pixel peak fit of the correlation, a least-square gaussian fit of 3×3 points is applied. The time steps have been carefully selected in order to achieve an optimal particle displacement (5-8 pixels per time-step) and range from 40 ms (on the surface) to 400 ms (maximal depth, $h = 5$ mm), which correspond to one and ten Faraday wave periods, respectively. Finally, the results are validated by imposing to neighbouring nodes a maximal displacement difference of 3.5 pixels, and the outlier replacement scheme (for the multi-grid interrogation) is set up to investigate lower-order peaks for five validation passes.

3 Results and Discussion

In the current experiments, PIV measurements of the Faraday flow have been carried out on the surface and at different depths in the water. PIV data is computed on grids with different refinement levels and time intervals. The analysis of the results is focused on the evolution of velocity fields, size of recirculation and vortex structures, as well as gradient-based variables (e.g. vorticity) at different water heights. Although the $z-$component (normal to the planes) of velocity could not be reconstructed from the available set-up, this approach was followed to highlight regions of interest for future, more elaborated 3D investigation. For the following figures and diagrams, the notation $\mathbf{u} = (u, v)^\top$ will be used to denote the velocity field and its components in $x-$ and $y-$direction respectively, and h will be used for the height of the measurement plane with respect to the container bottom.

Velocity fields

Fig. 2 shows an example of PIV evaluation at the water surface. The entire field of view is presented in Fig. 2(a), whereas Fig. 2(b) shows an enlarged region. The background is a mean of 10 successive experimental frames and provides visual validation of the PIV calculations (note the white traces left by the

particles movement). From the velocity field, a few characteristics of the Faraday flow can easily be recognised, namely the presence of counter-rotating vortex pairs with variable length scales, as it was observed by (von Kameke et al., 2011), as well regions of jet-like flow that are typically located between these vortex pairs. In this jet-like structures the flow is considerably accelerated. The structure of the Faraday waves can also be appreciated. This highlights the possibility of implementing a simultaneous measurement of the water height in order to couple the planar velocity field with the wave displacement. Additionally, it can be seen that, the Faraday wavelength λ_f is approximately 4 to 5 mm, which in turn validates the deep-water assumption. The vortex structures have a diameter of 1 to 2 Faraday wavelengths.

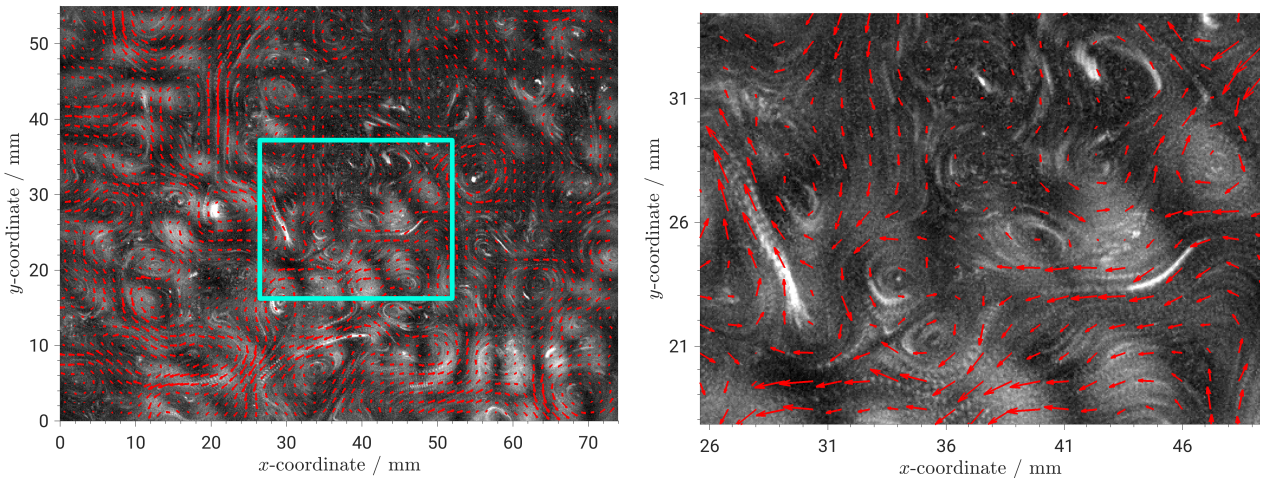

(a) (b)

Figure 2: Representation of an instantaneous velocity field (red vectors, every second vector depicted) overlapping the corresponding time-averaged raw data. Fig 2(a): Conversion factor: 18.94 px/mm, absolute velocity $|\mathbf{u}|$ ranging from 0 to 22.52 mm/s, with maximum in the streamlined structures. Fig 2(b): Enlargement of the cyan region to highlight particle traces. The presence of multiple counter-rotating vortex structures of different spatial scales can be appreciated. Jet-like flow develops between these vortices. Note that the pattern of surface waves can still be recognized.

Fig. 3 depicts the root-mean-square (RMS) values of u and v-velocity components and absolute velocity at the different measurement planes. The values have been averaged over all the available time steps. A dramatic difference can be appreciated for the RMS values of velocity at the surface and beneath it for both u and v. Interestingly, at the surface the flow presents symmetric RMS values in both directions (approximately 5 mm/s), whereas more pronounced differences appear at lower measurement heights, with the $u-$component being generally smaller. However, this is related to the chosen time scale and the of field-of-view. Either a larger region or longer averaging time should be inspected in order to capture the fluctuations larger and slower structures that develop beneath the surface.
Additionally, it can be noted that the velocity RMS values show a slight recovery below the half height of the water level ($h = 15$ mm). This phenomenon could be attributed to the vertical direction of the shaking, causing vertical streams in the normal direction being forced to deviate to the horizontal one as they impinge on the container bottom (as in a stagnation point flow). By observing the trend depicted in Fig. 3, it is clear that additional attention should be dedicated to the thin region (5 mm) right below the water surface, in order to more accurately describe the steep reduction in RMS velocities, and the corresponding evolution of the underlying flow structures. Furthermore, additional measurements in the region close to the container bottom could reveal the full extent of the observed recovery in RMS velocity values. The error bars in Fig. 3 show the standard deviation of the time-averaged signals. The confidence interval at the surface is considerably larger as the flow is faster and more chaotic.

The time-averaged velocity distributions are depicted in Fig. 4 for the water surface and the deepest plane ($h = 5$ mm from the bottom). A rather symmetric flow condition can be seen at the surface, where both u (red) and v (blue) are symmetric to 0 and show similar deviation and peak values and follow Gaussian distribution. There is a substantial difference at the bottom of the container for $h = 5$ mm, where v shows a

clear bias towards positive values, and for which the bin counter is considerably larger than for u-velocities. As mentioned before, this could be attributed to the presence of even larger structures that could not be captured with the current field of view and averaging time.

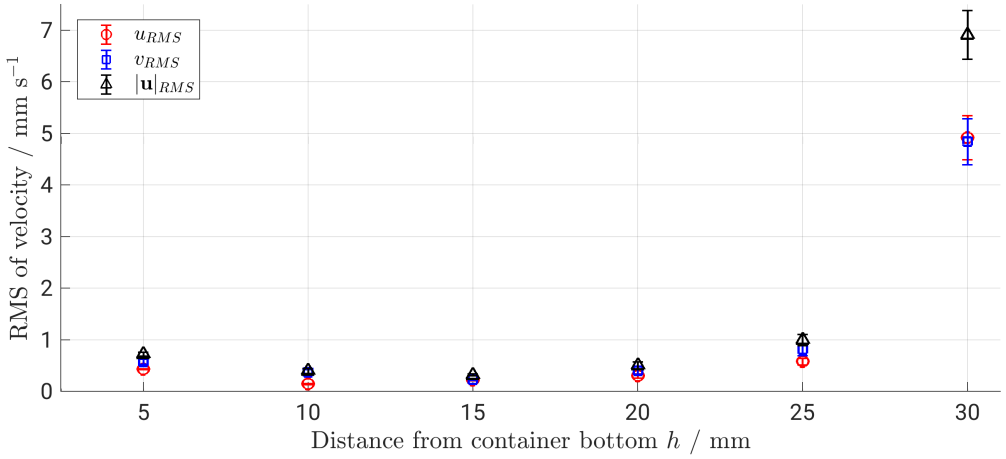

Figure 3: Evolution of the RMS of velocity components at different heights. Values averaged over all the time steps, with error bars showing the standard deviation. A dramatic reduction in all the values can be observed in the 5 mm region right below the surface. At depths below the container half-height, a slight recovery in RMS values can be appreciated.

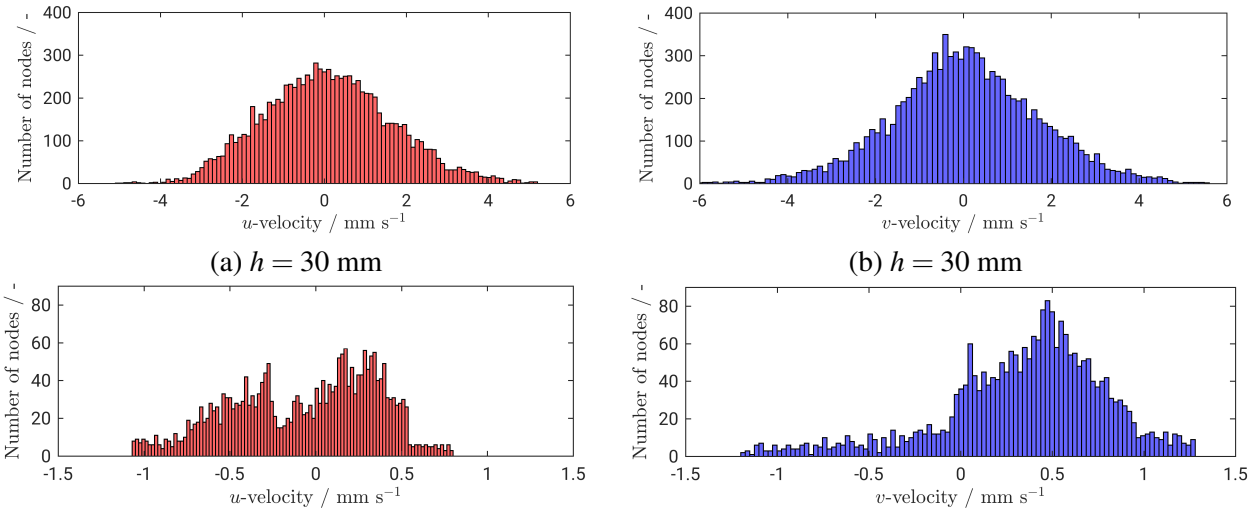

(a) $h = 30$ mm (b) $h = 30$ mm

(c) $h = 5$ mm (d) $h = 5$ mm

Figure 4: Time-averaged velocity distributions for u (red) and v (blue), at the water surface (a, b) and close to the container bottom (c, d). The symmetry of the velocity distribution can be appreciated for the measurements at the wave surface, and asymmetry prevails in the water volume. All distributions show velocity values divided in 100 bins. Magnitude and number of counters vary according to height and grid spacing.

Flow vorticity

A very useful tool to further investigate the relative size and behaviour of the ordered structured in 2D turbulence is the flow vorticity, computed for the 2D case as $\omega_z = \partial v/\partial x - \partial u/\partial y$. In Fig. 5, an example of vorticity contours are presented for an instantaneous time step (after 4 s of measurements) at four different heights.

The results reflect the considerations regarding the RMS values of velocities, and the expectations regarding

the behaviour of the structures sizes and vorticity intensity. On the wave surface (Fig. 5 (a)), regions of alternating vorticity are densely distributed across the entire field of view, and jet-like flow structures develop between fast, counter-rotating vortices (mostly along the white-colored boundaries). Immediately below the surface, the vorticity intensity drops significantly (more than one order of magnitude), as shown in Fig. 5 (b). Structures with local peaks in vorticity are still present, but more sparsely and in a less coherent order. Right below the surface, the planar velocity field is strongly impacted by the vertical oscillation at the surface. The Faraday ripples provide thus vertical oscillatory energy through a structure of oscillating solitons, which was denoted as the 'turbulent fuel' in Francois et al. (2014). Interestingly, although the phenomenon of 2D turbulence is localized at the surface, energy is also transferred to the lower layers of the fluid, where larger and slower-rotating structures seem to be formed, as indicated by the vorticity planes in Fig. 5 (c) and (d).

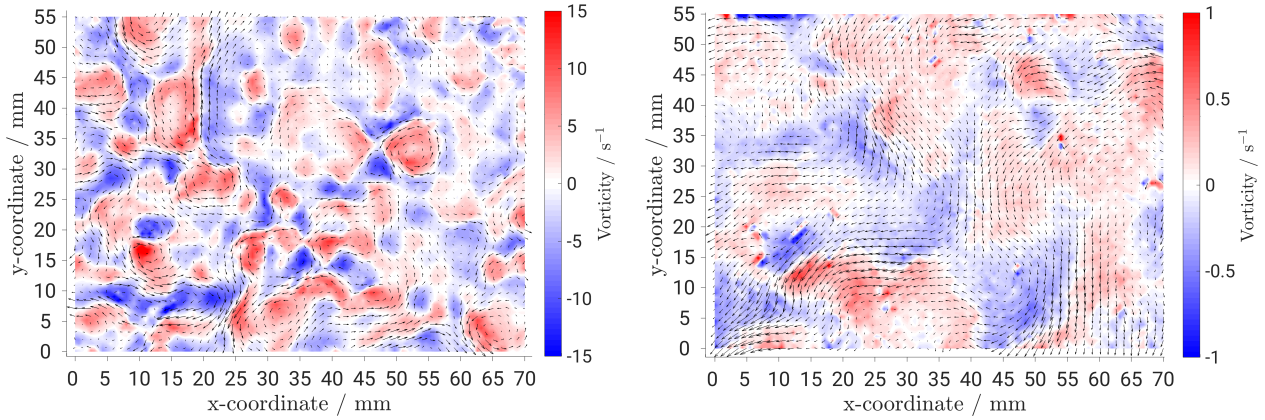

(a) $h = 30$ mm

(b) $h = 25$ mm

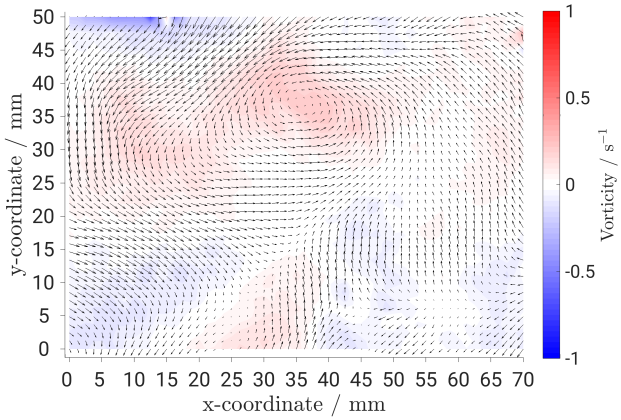

(c) $h = 15$ mm

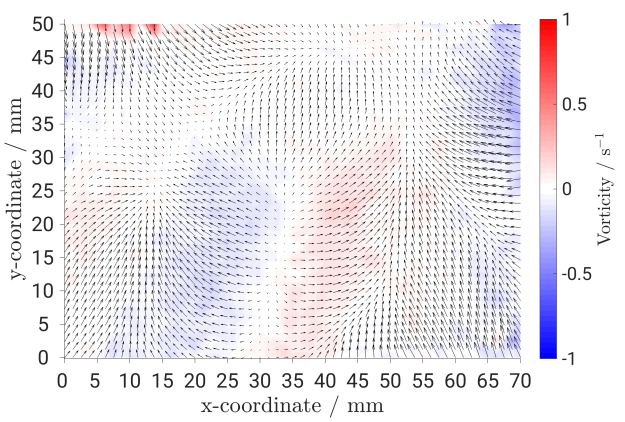

(d) $h = 5$ mm

Figure 5: Instantaneous vorticity fields at four different heights. Vorticity computed as $\omega_z = \partial v/\partial x - \partial u/\partial y$ from reconstructed gradients in physical units (mm). Note the different scales between values at the surface (Fig. 5 (a)) and at different depths in the water volume. Black arrows qualitatively depict the local velocity field (size is not scaled across the four figures).

4 Conclusions

The Faraday experiment has been recreated in a circular container (diameter 290 mm) filled with up to a height of 30 mm of water. The container was vertically agitated with monochromatic forcing at a frequency $f_0 = 50$ Hz and at the threshold acceleration $a_{th} = 0.466$ g. 2D-velocity fields have been measured with PIV techniques on the surface and at different horizontal planes in the water. The results of this experiment have highlighted interesting flow features developing beneath the surface of a Faraday wavefield, which guide the

attention for future investigations.
A lattice of counter-rotating vortices has been found on the water surface. The vortices have a diameter ranging from one to two Faraday wavelengths. Furthermore, jet-like structures have been found between these vortices, where the flow is accelerating and shows peaks of absolute velocity.
By analysing the mean RMS values of the velocity components and magnitude at different heights, it has been shown that within the water volume the flow is considerably slower than on the surface (which suggests that Faraday flow condition are localized on the surface or in a small layer below it). Below half depth of the water, a slight recovery in RMS values can be appreciated, which might be related to vertical components of the flow being forced in the horizontal direction by the presence of the bottom wall.
The analysis of the mean velocity distribution showed, as expected, a rather symmetric flow condition on the water surface. At further depths however, asymmetric distributions in velocity support the claim that larger and slower structures develop, which are not entirely resolved with the selected field of view and temporal averaging.
Results for instantaneous vorticity distribution and overlapping velocity fields highlight the presence of rotational flow at different depths. However, it has been shown that ordered structures are localised at the surface, and that the vorticity intensity drastically decreases right below it. Nevertheless, a strong vertical motion is present at the immersed planes, which has been neglected so far.

Outlook

In regard to the obtained results, the following steps will be undertaken in order to further investigate the sub-surface velocity in Faraday flows.
A larger field of view will be considered in order to possibly resolve the length-scales of the larger structures to characterise the flow developing at different heights beneath the surface of Faraday ripples. Similarly, Planar PIV will be used to characterise the vertical component of velocity and to see to which extent the vertical motion of the surface liquid expands in the volume of water.
Experiments with different boundary and forcing conditions (driving amplitude, frequency, water height) will be considered to investigate the trend highlighted by the values of RMS velocities, in particular close to the container bottom and right beneath the surface.
Furthermore, the measurement technique will be improved by using time-resolved scanning (TRS) techniques for PIV. This would allow to simultaneously scan different planes and better couple the velocity fields at different heights. For the surface measurements, PIV will be coupled with wave-surface reconstruction to better describe the creation of horizontal vortex structures through vertical agitation.
Finally, stereo PIV will be used in order further resolve the flow features by adding information about the z-component of velocity.

Acknowledgements

The authors gratefully acknowledge the financial support provided by the Deutsche Forschungsgemeinschaft (DFG) within the project 395843083 (KA 4854/1-1). We thank Ms. Nikki Indresh Lal for the aid with the experimental set-up.

References

Biferale L, Buzzicotti M, and Linkmann M (2017) From two-dimensional to three-dimensional turbulence through two-dimensional three-component flows. *Physics of Fluids* 29:111101

Boffetta G and Ecke RE (2012) Two-dimensional turbulence. *Annual Review of Fluid Mechanics* 44:427–451

Couder Y, Protiere S, Fort E, and Boudaoud A (2005) Dynamical phenomena: Walking and orbiting droplets. *Nature* 437:208

Faraday M (1831) Xvii. on a peculiar class of acoustical figures; and on certain forms assumed by groups of particles upon vibrating elastic surfaces. *Philosophical transactions of the Royal Society of London* 121:299–340

Farazmand MM, Kevlahan NR, and Protas B (2011) Controlling the dual cascade of two-dimensional turbulence. *Journal of Fluid Mechanics* 668:202–222

Francois N, Xia H, Punzmann H, Ramsden S, and Shats M (2014) Three-dimensional fluid motion in faraday waves: creation of vorticity and generation of two-dimensional turbulence. *Physical Review X* 4:021021

Francois N, Xia H, Punzmann H, and Shats M (2013) Inverse energy cascade and emergence of large coherent vortices in turbulence driven by faraday waves. *Physical review letters* 110:194501

Kraichnan RH (1971) Inertial-range transfer in two-and three-dimensional turbulence. *Journal of Fluid Mechanics* 47:525–535

Ramshankar R, Berlin D, and Gollub JP (1990) Transport by capillary waves. part i. particle trajectories. *Physics of Fluids A: Fluid Dynamics* 2:1955–1965

Saylor J and Kinard A (2005) Simulation of particle deposition beneath faraday waves in thin liquid films. *Physics of Fluids* 17:047106

von Kameke A, Huhn F, Fernández-García G, Munuzuri A, and Pérez-Muñuzuri V (2011) Double cascade turbulence and richardson dispersion in a horizontal fluid flow induced by faraday waves. *Physical review letters* 107:074502

von Kameke A, Huhn F, Munuzuri A, and Pérez-Muñuzuri V (2013) Measurement of large spiral and target waves in chemical reaction-diffusion-advection systems: Turbulent diffusion enhances pattern formation. *Physical review letters* 110:088302